Molecular Cancer Therapeutics

Antitumor Activity of Osimertinib, an Irreversible Mutant-Selective EGFR Tyrosine Kinase Inhibitor, in NSCLC Harboring EGFR Exon 20 Insertions

Nicolas Floc'h[1], Matthew J. Martin[1], Jonathan W. Riess[2], Jonathan P. Orme[3], Anna D. Staniszewska[1], Ludovic Ménard[1], Maria Emanuela Cuomo[3], Daniel J. O'Neill[3], Richard A. Ward[1], M. Raymond V. Finlay[1], Darren McKerrecher[1], Mingshan Cheng[4], Daniel P. Vang[2], Rebekah A. Burich[2], James G. Keck[4], David R. Gandara[2], Philip C. Mack[2], and Darren A.E. Cross[1]

Abstract

EGFR exon 20 insertions (Ex20Ins) account for 4% to 10% of EGFR activating mutations in non–small cell lung cancer (NSCLC). EGFR Ex20Ins tumors are generally unresponsive to first- and second-generation EGFR inhibitors, and current standard of care for NSCLC patients with EGFR Ex20Ins is conventional cytotoxic chemotherapy. Therefore, the development of an EGFR TKI that can more effectively target NSCLC with EGFR Ex20Ins mutations represents a major advance for this patient subset. Osimertinib is a third-generation EGFR TKI approved for the treatment of advanced NSCLC harboring EGFR T790M; however, the activity of osimertinib in EGFR Ex20Ins NSCLC has yet to be fully assessed. Using CRISPR-Cas 9 engineered cell lines carrying the most prevalent Ex20Ins mutations, namely Ex20Ins D770_N771InsSVD (22%) or Ex20Ins V769_D770InsASV (17%), and a series of patient-derived xenografts, we have characterized osimertinib and AZ5104 (a circulating metabolite of osimertinib) activities against NSCLC harboring Ex20Ins. We report that osimertinib and AZ5104 inhibit signaling pathways and cellular growth in Ex20Ins mutant cell lines *in vitro* and demonstrate sustained tumor growth inhibition of EGFR-mutant tumor xenograft harboring the most prevalent Ex20Ins *in vivo*. The antitumor activity of osimertinib and AZ5104 in NSCLC harboring EGFR Ex20Ins is further described herein using a series of patient-derived xenograft models. Together these data support clinical testing of osimertinib in patients with EGFR Ex20Ins NSCLC. *Mol Cancer Ther; 17(5); 885–96. ©2018 AACR.*

Introduction

EGFR Exon 20 insertions (Ex20Ins) collectively comprise the third most common category of EGFR activating mutations found in non–small cell lung cancer (NSCLC) following the canonical in-frame deletions in exon 19 (Ex19del) and the L858R point mutation in exon 21. These two mutations represent approximately 90% of all EGFR mutations (1), whereas EGFR Ex20Ins account for 4% to 10% of all EGFR mutant NSCLC (2–4).

Ex20Ins mutations represent a combination of in-frame insertions and/or duplications, and to date more than 100 different variations have been described (4). Most of the Ex20Ins mutations are located close to the end of the C-helix domain within the N-lobe of the kinase, after residue M766, but a small number map to the middle of the C-helix (4). The molecular mechanisms underpinning Ex20Ins tumorigenicity remain poorly understood, compounded by the lack of disease-relevant model systems.

Unlike Ex19del and L858R, most of the Ex20Ins mutations have been associated in preclinical and clinical studies with *de novo* resistance to the currently approved first-line EGFR-tyrosine kinase inhibitors (TKI), erlotinib, gefitinib, and afatinib (2, 4–8). The rare A763_Y764insFQEA mutation (6% prevalence across the Ex20Ins segment) is the only Ex20ins reported to be clinically sensitive to these TKIs (9).

Advanced NSCLC currently continues to have a poor long-term prognosis despite recent advances with 5-year overall survival less than 5% (10). Median survival is improved in NSCLC patients with oncogenic driver mutations (11). However, for EGFR Ex20Ins, the standard of care remains conventional cytotoxic therapies similar to the treatment of EGFR wild-type tumors. Nevertheless, lung adenocarcinomas are likely as dependent on EGFR Ex20Ins as they are on other transforming EGFR mutations for their growth and survival. Therefore, development of EGFR-TKIs that can more effectively target NSCLC with EGFR Ex20Ins mutations represents a significant advance for patients with this genotype.

Osimertinib is a next-generation EGFR TKI with activity against both canonical activating and T790M mutant forms of EGFR, and has gained approval (including in the United States, Europe, and Japan) for the treatment of T790M-positive advanced NSCLC

[1]IMED Oncology, AstraZeneca, Cambridge, Cambridgeshire, United Kingdom. [2]University of California Davis Comprehensive Cancer Center, Sacramento, California. [3]IMED Discovery science, AstraZeneca, Cambridge, Cambridgeshire, United Kingdom. [4]Jackson Laboratory West, Sacramento, California.

Note: Supplementary data for this article are available at Molecular Cancer Therapeutics Online (http://mct.aacrjournals.org/).

N. Floc'h, M.J. Martin, and J.W. Riess have contributed equally and should be considered as co-first authors.

Corresponding Authors: Nicolas Floc'h, AstraZeneca, Robinson Way, Cambridge CB2 0RE, United Kingdom. Phone: 012-2376-9654; E-mail: nicolas.floch@astrazeneca.com and Darren A.E. Cross, Astrazeneca, Robinson Way, Cambridge CB2 0RE, United Kingdom. Phone: 078-768-75414; E-mail: darren.cross@astrazeneca.com

doi: 10.1158/1535-7163.MCT-17-0758

(12, 13). However, osimertinib's potential in the EGFR Ex20Ins patient population remains to be fully assessed. Some recent *in vitro* work using Ba/F3 stable cell lines suggested that osimertinib could be potent against some Ex20Ins mutations (14), but this study did not examine activity in more disease-relevant models, nor did it evaluate *in vivo* activity.

The work presented herein demonstrates that osimertinib has the potential to improve upon the current treatment options for NSCLC patients whose tumors harbor an Ex20Ins mutation, and warrants its further clinical investigation.

Materials and Methods

Cell lines

Cos-7 cells were obtained from European Collection of Authenticated Cell Cultures (ECACC). NCI-H2073 (H2073) were obtained from ATCC. The H2073 were derived from a stage IV adenocarcinoma (NSCLC). Cos-7 cells were cultured in DMEM (Sigma-Aldrich) supplemented with 10% FCS (PAA) and 1% Glutamax (Life Technologies). H2073 cells were cultured in RPMI1640 (Sigma-Aldrich) supplemented with 10% FCS and 1% Glutamax or 2 mmol/L L-glutamine. All cell lines were authenticated at AstraZeneca cell banking using DNA fingerprinting short tandem repeat (STR) assays and confirmed to be free of bacterial and viral contaminations by IDEXX. All cell lines were used within 15 passages, and less than 6 months.

Compounds

Osimertinib, AZ5104, and Afatinib were synthetized by AstraZeneca. The synthesis and structures of osimertinib and AZ5104 have been previously reported as compounds 8 and 27 in ref. 12.

CRISPR cell-line generation

For the genome editing, H2073 cells harboring wt-EGFR were transfected by electroporation following a standard Neon protocol with a plasmid encoding both Cas9-T2A-GFP and a guide specific to the Exon 20 insertion site (CACGTGGGGGTTGTCCACGC). A synthetic single-strand DNA oligo donor with homology arms to EGFR Exon20 and the required oligonucleotides insertion was added to the transfection mix in a ratio of 100:1 to the plasmid molarity. Oligo donors were designed to harbor a silent mutation in the PAM site and a silent mutation generating a restriction site for screening purposes (ASV: GAAGCCTACGTGATGGCCAGCGTGGCCAGCGTGGAC AACCCCCACGTGTGCCGCCTGCTGGGCATCT; SVD: GAAGCCTACGTGATGGCCAGC GTGGACAGCGTGGACAACCCCCACGTGTGCCGCCTGCTGGGCATCT).

Transfected cells were grown in the presence of 10 nmol/L afatinib for 2 weeks, before single cell cloning. Single cell clones were grown in 96-wells, DNA extracted by alkyline lysis and analyzed by ddPCR with specific probes. Clones positive for the specific insertion and negative for wt alleles were then sequenced to confirm the correct genome edit by Sanger sequencing.

Cell transfection

Cos-7 cells were transiently transfected using pcDNA3.1-D770_N771InsNPG (NPG), D770_N771InsSVD (SVD), V769_D770InsASV (ASV), and A763_Y764insFQEA (FQEA) constructs obtained from GeneArt. Transfections were carried out using MaxCyte electroporation with cells being frozen 24 hours posttransfection.

For siRNA experiments, H2073 cells expressing wt-EGFR, Ex20InsSVD, or Ex20InsASV were plated in six-well dishes at 250,000 cells/well overnight followed by transfection the following day. siRNAs were complexed with 5 μL/well lipofectamine RNAimax (Invitrogen) and incubated with cells at a final concentration of 10 nmol/L. siRNAs used (all siRNAs Dharmacon ON-TARGETplus) were siEGFR-1 (J-003114-12), siEGFR-2 (J-003114-13), single control siRNA (D-001810-01), or pooled control (D-001810-10). After 48 hours cells were either lysed for Western blotting or plated in for growth experiments. Cells were plated at 2,500 cells/well in 96-well, whitesided dishes. Cells were analyzed 96 hours later using Cell Titer-Glo reagent (Promega) as per the manufacturer's instructions. Values were normalized to control siRNA and plotted using GraphPad Prism. Experiments were repeated for a minimum $n = 3$.

In vitro EGFR phosphorylation assays

EGFR phosphorylation was measured using a modified Cisbio Pan phospho-EGFR Cellular Assay Kit. All Cos-7 cells were revived in culture flasks for 16 hours in DMEM supplemented with 10% FCS. For Cos-7 ASV and SVD cells medium was replaced with DMEM supplemented with 3% charcoal stripped FCS for the final 2 hours. Cos-7 cell and H2073 were detached using TrypLE Express Enzyme (Life Technologies) from culture flasks and resuspended, 5 μL of cell suspension at densities between 600 and 1,400 cells per well were dispensed into a Greiner low volume 384 proxi plates pre-dosed with titrations of test compound and incubated for 2 hours at room temperature. The H2073, Cos-7 ASV, and SVD cells were stimulated for the final 10 minutes with 200 ng/mL of EGF. Following the 2-hour incubation, 2 μL of the XL665 and Cryptate labeled antibodies diluted in lysis buffer were added to the cells and incubated for 2 hours at room temperature. Plates were then read on Pherastar with a HTRF module. IC_{50} values were determined following 2-hour incubation with compound titrations. Data were exported to Genedata Screener software package (Genedata) to generate sigmoidal dose–response curves, an IC_{50} value was generated by determining the compound concentration at which there was a 50% inhibition in signal.

Proliferation assay

H2073, H2073-SVD, and H2073-ASV cells were plated in 384-well plates at a density between 2,500 and 3,000 cells per well, depending on the cell line, in 40 μL per well of RPMI1640 media containing 10% FCS, 1% glutamax. The cells were allowed to attach overnight at 37°C under 5% CO_2. The following day, titrations of test compound were added to the assay plates using an Echo Liquid Handler Labcyte, and the treated cells were incubated for a further 6 days at 37°C under 5% CO_2. Following the 6-day incubation, 5 μL of 2 μmol/L SYTOX Green Nucleic Acid Stain (Life Technologies) and 10 μL of 0.25% saponin (Sigma) was added per well, and the plates were incubated at room temperature for 5 hours. The number of fluorescent cells per well was measured on a CellInsight.

Cell viability and apoptosis assays

Cells were plated in white-sided 96-well plates at 2,500 cells/well in 100 μL of media. Twenty-four hours later, cells were treated in duplicate with a nine-point half-log dosing as well as a DMSO control using the HP D300 Digital Dispenser (Hewlett-Packard). Ninety-six hours after dosing cells were analyzed using Cell Titer-

Glo reagent (Promega) as per the manufacturer's instructions. Values were normalized to DMSO control and plotted using GraphPad Prism. Experiments were repeated for a minimum $n = 3$, and presented graphs represent a typical growth curve. For apoptosis measurement, cells were transfected with EGFR siRNA as above and plated in 96-well plates at 5,000 cells/well. Forty-eight hours after plating, cells were analyzed using the Caspase 3/7-Glo reagent (Promega) as per the manufacturer's instructions. Duplicate plates were analyzed for cell viability by Cell Titer-Glo simultaneously, and caspase values were normalized to average viability for each treatment. Graphs represent values relative to DMSO $n = 3$. For serum titration experiments, cells were plated at 2,500 cells/well in RPMI containing either 1% or 10% FCS. Twenty-four hours after cell plating, a subset of wells were analyzed using Cell Titer-Glo (Day 0), whereas an additional subset of cells cultured in 1% FCS were treated with 50 ng/mL EGF (Preprotech). Ninety-six hours later (Day 4), all remaining wells were analyzed using Cell Titer-Glo, and such data are represented as increase in viability values from Day 0 to Day 4 ($n = 3$ separate experiments). For each of these experiments, statistical significance was evaluated by a two-tailed *t* test.

Immunofluorescence and confocal microscopy analyses

Cells were plated in 24-well plates (5×10^4 per well) onto glass coverslips and stimulated or not the following day in full medium as indicated and fixed in 4% PFA for 10 minutes. Free aldehydes were quenched with 50 mmol/L NH4Cl in PBS for 10 minutes. Fixed cells were permeabilized in 0.1% Triton X-100 in PBS/2% BSA for 15 minutes and then incubated at room temperature for 30 minutes with the primary antibodies. Cells were rinsed and incubated with appropriate secondary antibodies for 30 minutes. Cells were washed three times in PBS and once in water and then mounted in DAPI-containing mounting medium (Thermofisher). All images were acquired using a confocal laser scanning microscope (Leica TCS SP5) equipped with a 63 × oil immersion objective. Alexa Fluor 488 was excited with the 488-nm line of an Argon laser, Alexa Fluor 555, and TRITC were excited with a 543-nm HeNe laser. Each image corresponds to a single section of 0.8 μm thickness.

Xenograft studies

All animal studies were conducted in accordance with U.K. Home Office legislation, the Animal Scientific Procedures Act 1986, and the AstraZeneca Global Bioethics policy. All experimental work is outlined in project license 70/8894, which has gone through the AstraZeneca Ethical Review Process. Studies in the United States were conducted in accordance with the guidelines established by the internal Institutional Animal Care and Use Committee (IACUC) and reported following the ARRIVE (Animal Research: Reporting In Vivo Experiments) guidelines. Randomization of animals onto study was based on initial tumor volumes to ensure equal distribution across groups. A power analysis was performed whereby group sizes were calculated to enable statistically robust detection of tumor growth inhibition ($\geq$5 per group) or pharmacodynamic endpoint ($\geq$4 per group).

Human H2073 parental, H2073-SVD, and H2073-ASV cell lines were cultured in RPMI1640 supplemented with 20% (v/v) FCS and 1% (v/v) glutamine and cultured in a humidified incubator with 5% CO_2 at 37°C. H2073-WT, -SVD, and -ASV xenografts were established by subcutaneous implantation of 1×10^7, cells per animal, in 100 μL of cell suspension including 50% matrigel, into the dorsal left flank of female SCID mice. All mice were older than 6 weeks at the time of cell implant. Tumor growth was monitored twice weekly by bilateral caliper measurements and tumor volume calculated using elliptical formula (pi/6 × width × width × length).

For the LXF2478 (Oncotest) and LU0387 (Crown Bioscience) PDX models, tumor fragments from donor mice inoculated with primary human lung cancer tissues were harvested and inoculated subcutaneously into the left and right flank respectively of female nude mice for LXF2478 and LU0387. Tumor growth was monitored twice weekly by bilateral caliper measurements and tumor volume calculated using the formula $0.5a \times b^2$ (where *a* and *b* are the long and short diameters of the tumor, respectively).

Mice were randomized into vehicle or treatment groups with approximate mean start size of 0.2 cm^3. Randomization for animal studies was based on initial tumor volumes to ensure equal distribution across groups. Mice were dosed daily by oral gavage for the duration of the treatment period with vehicle, osimertinib, AZ5104, or afatinib. Tumor growth inhibition (%TGI) from the start of treatment was assessed by comparison of the geometric mean change in tumor volume for the control and treated groups using the formula: $\%TGI = (1 - \{Tt/T0/Ct/C0\}/1 - \{C0/Ct\}) \times 100$, where Tt is the geo mean tumor volume of treated at time *t*, T0 is the geo mean tumor volume of treated at time 0, Ct is the geo mean tumor volume of control at time *t*, and C0 is the geo mean tumor volume of control at time 0. Tumor regression was calculated as the percentage reduction in tumor volume from baseline value: $\%\ regression = (1 - RTV) \times 100\%$, where RTV is the mean relative tumor volume. Statistical significance was evaluated using a one-tailed *t* test.

For pharmacodynamic studies, mice were randomized at a tumor volume between 0.2 and 0.7 cm^3 using the same randomization criteria as the tumor growth inhibition studies. Mice were then treated orally with a single bolus dose of either vehicle, osimertinib, AZ5104, or afatinib. Tumors were excised at specific time points after dosing and flash frozen in liquid nitrogen.

In all *in vivo* studies, osimertinib, AZ5104, and afatinib were administered via oral gavage. Osimertinib, AZ5104, and afatinib were suspended in 0.5% HPMC, 1% polysorbate 80, and 0.5% HPMC + 0.1% polysorbate 80, respectively.

Immunoblotting

For *in vitro* immunoblots, culture medium was aspirated from cells and cells were washed once in cold PBS. Cells were scraped into 100 μL lysis buffer [25 mmol/L Tris-HCl (pH 6.8), 3 mmol/L EDTA, 3 mmol/L EGTA, 0.27 M sucrose, 0.5% Triton X-100, 50 mmol/L NaF, 2 mmol/L Na_3VO_4, 10 mmol/L β-glycerophosphate, 5 mmol/L sodium pyrophosphate, complete protease inhibitor tablets (Roche) per 35 mm dish].

For *ex vivo*, H2073 CRISPR PD samples, pea-sized fragments of xenograft tissue were homogenized in the FastPrep-24 5G instrument (MP Bio) in lysis buffer (same as above + 0.1% β-mercaptoethanol) supplemented with protease and phosphatase inhibitor cocktails (Sigma). Homogenates were briefly sonicated using Diagenode Bioruptor plus before 10-minute centrifugation and protein quantification with Pierce protein assay (Thermofisher). For all samples, equal protein amounts were loaded for SDS-PAGE using 4% to 12% gradient Bis-Tris precast gels (Novex Life Technologies), followed by transfer to nitrocellulose membranes using the iBlot2 dry transfer system (Novex Life Technologies). After blocking in 5% milk-TBST, membranes were blotted with

phospho-AKT (Ser473; Cell Signaling Technology; 4060), total AKT (tAKT; Cell Signaling Technology; 9272), phospho-ERK (Thr202/Tyr204; Cell Signaling Technology; 9101), total ERK (tERK; Cell Signaling Technology; 9102), phospho-EGFR (Tyr1068; Cell Signaling Technology; 2234), total EGFR (tEGFR; Cell Signaling Technology; 2232), phospho-S6RP (Ser235/236; Cell Signaling Technology; 4858), total S6RP t(S6RP) (Cell Signaling Technology; 2217), phospho-Stat3 (Tyr705; Cell Signaling Technology; 9145), total Stat3 (tStat3; Cell Signaling Technology; 9139), GAPDH (Cell Signaling Technology; 2118), or vinculin (Abcam; ab18058) followed by horseradish peroxidase (HRP)–conjugated secondary antibodies (Cell Signaling Technology; 7074 or 7076). Signals were detected with SuperSignal West Dura or Pico detection reagents (ThermoFisher). Western blots were developed using G:Box chemigeuous instrument (Syngene) or on Amersham Hyperfilm ECL (GE Healthcare) and where indicated, signal was quantified in Syngene Genetools software. Protein levels were then normalized to the levels of loading control (vinculin) and treatment groups were normalized to the mean of time-matched vehicle groups. Statistical significance was evaluated using a one-way, two-sided ANOVA.

ELISA

Assays to measure general Tyrosine-phosphorylation and total levels of endogenous EGFR in xenograft tissues were carried out according to the protocol described in the R&D Systems DuoSet IC Human PhosphoEGFR ELISA and DuoSet IC Human Total EGFR ELISA (R&D Systems, nos. DYC1095 and DYC1854). Xenograft lysates were obtained and protein levels were quantified as described in the immunoblotting section. Nunc black MaxiSorp 96-well plates were coated with capture antibody and then blocked with SuperBlock buffer (ThermoFisher). Following the removal of the blocking solution, 50 µL of lysate (for pEGFR assay 3 µg of protein from H2073-SVD or 2 µg of protein from H2073-ASV; for tEGFR assay 0.75 µg of protein from H2073-SVD or 0.4 µg of protein from H2073-ASV) was transferred to the Nunc black MaxiSorp 96-well plates and incubated for 2 hours. Following aspiration and washing of the plates with PBST, 50 µL of detection antibody was added and incubated for 2 hours. Following aspiration and washing of the plates with PBST, 50 µL of Streptavidin-HRP was added to the tEGFR assay and incubated for 20 minutes in darkness. Following aspiration and washing of the plates with PBST. Fifty microliters of QuantaBlu fluorogenic peroxidase substrate (ThermoFisher) was added and incubated for 5 minutes. Fluorescence was read immediately afterwards on an Saffire plate reader using an excitation wavelength of 325 nm and an emission wavelength of 420 nm. Phospho-Tyrosine EGFR and total EGFR levels were calculated based on standard curve included in the assays. Phospho-Tyrosine EGFR levels were normalized to total EGFR levels and treatment groups were normalized to the mean of time-matched vehicle groups. Statistical significance was evaluated using a one-way, two-sided ANOVA test.

Treatment of LG1423 patient-derived xenograft

The PDX LG1423 was derived from a pleural effusion of a patient harboring EGFR Ex20ins (V769_D770InsASV) following written informed consent on a UC Davis IRB approved protocol for creating patient PDX and using an established IACUC approved protocol at Jackson Laboratory West (Sacramento, CA). At the time of PDX creation the patient was EGFR-TKI naïve. The established xenograft was implanted subcutaneously into the right flank of NOD.Cg-PrkdcscidIl2rgtm1Wjl/SzJ (NSG) mice for tumor growth inhibition studies (TGI) with vehicle (No treatment), erlotinib (50 mg/kg p.o. daily; Roche/Genentech), afatinib (20 mg/kg/day P.O. daily; Boehringer Ingelheim), and osimertinib (25 mg/kg p.o. daily; AstraZeneca) administered by oral gavage for 21 days.

Pharmacodynamic studies of LG1423 patient-derived xenotransplant

Mice were allocated at a tumor volume in between 0.4 and 0.6 cm^3 to receive one dose of vehicle (no treatment), osimertinib, erlotinib, or afatinib. Tumors were excised at specific time points after dosing and flash frozen in liquid nitrogen. Results were analyzed by one-way ANOVA and Bonferonni's multiple comparison test using Graphpad Prizm 5.0 software.

For the *ex vivo* immunoblots, tumors were homogenized in 200 µL of PBS (pH 7.4) using a Benchmark D1000 homogenizer for 20 to 30 seconds followed by adding 600 µL of lysis buffer [25 mmol/L Tris-HCl (pH 7.4), 1 mmol/L EDTA, 1 mmol/L EGTA, 10 mmol/L NaF, 1% NP-40, 10% Glycerol, 2 mmol/L Na_3VO_4 (Sigma, S6508), and 1× protease inhibitors (Roche, 11836170001)]. Homogenates were flash frozen in liquid nitrogen, thawed on ice for a total of three freeze–thaw cycles. The homogenates were then centrifuged twice, transferring the lysate to fresh tubes after each centrifugation and protein quantification was performed using Pierce BCA (ThermoScientific, 23255). For SDS-PAGE, equal amounts of protein were loaded onto Mini-Protean 10% TGX precast gels (BioRad, 456-1036) as previously described (Holland et al.) and transferred onto 0.2 µm nitrocellulose membranes using a BioRad Trans-Blot Turbo transfer system and Trans-Blot Turbo Transfer Packs (BioRad, 170-4159). Membranes were blocked with 2% milk-TBST and blotted with phospho-EGFR (Invitrogen, 44788G), EGFR (Cell Signaling Technology, 2646), phospho-Akt (Cell Signaling Technology, 4060), Akt (Cell Signaling Technology, 9272), phospho-Erk (Cell Signaling Technology, 4370), Erk (Cell Signaling Technology, 4696), phospho-Stat3 (Cell Signaling Technology, 9145), Stat3 (Cell Signaling Technology, 9139), phospho-S6R (Cell Signaling Technology, 4858), S6R (Cell Signaling Technology, 2217), or Actin (Sigma, A5541) followed by HRP-conjugated secondary antibodies (Promega, W401B and W402B) and detection with WesternSure Premium Chemiluminescent Substrate (Li-Cor, 926-95000). Membranes were scanned and quantified using the C-Digit Blot Scanner (Li-Cor) and Image Studio Lite version 5.0 software. Results were analyzed by one-way ANOVA and Bonferonni's multiple comparison test using Graphpad Prizm 5.0 software.

Results

Characterization of the activity of the Exon 20 insertion mutations

To better understand the activating potential and the drug sensitivity of Ex20Ins mutations to EGFR TKIs, we used CRISPR editing technology to replace the wild-type (wt) EGFR alleles of the H2073 cell line (H2073-WT) with either Ex20Ins D770_N771InsSVD (H2073-SVD) or Ex20Ins V769_D770InsASV (H2073-ASV) variants, the two most prevalent forms of Ex20Ins, which account for approximately 40% of such patients (Supplementary Fig. S1A and S1B).

When cultured in 1% serum condition, the H2073-SVD and H2073-ASV cell lines grew independently of the addition of

exogenous EGF, whereas the H2073-WT parental cell line was unable to proliferate in the absence of EGF (Fig. 1A). The proliferation of parental cells was stimulated by both EGF and serum treatment; however, these factors were unable to increase proliferation of the Exon20 insert mutants over 1% serum conditions, indicating that maximal proliferation occurs in this low serum context. This Exon20 insert-driven growth phenotype correlates with sustained EGFR pathway activation in low serum, shown in Fig. 1B. As demonstrated previously using EGFR TKI (13) or using siRNA against EGFR (Supplementary Fig. S2A), the survival of H2073-WT cell line is dependent on EGFR. Similarly, siRNA knockdown of EGFR inhibited the survival of both H2073-SVD and -ASV cell lines (Supplementary Fig. S2A). Accordingly, EGFR knockdown in these cells strongly inhibited signaling through the RAS/MAPK pathway (Supplementary Fig. S2B) and induced caspase activation relative to control siRNA (Supplementary Fig. S2C). To gain further insight into the biological impact of these prevalent Ex20Ins mutations, and because the impact on receptor localization has not been reported, we used confocal microscopy to compare Ex20Ins mutant biology to wt-EGFR. As expected, wt-EGFR was mostly located at the plasma membrane in the H2073-WT cells in the absence of ligand stimulation. However, in contrast, in both the H2073-SVD and H2073-ASV cell lines, EGF receptor appears to be constitutively internalized and colocalized with EEA1, a marker of the early endosome (Fig. 1C). Altered EGFR localization suggests that endosomal signaling of EGFR Ex20ins may be an important mechanism regulating EGFR-dependent tumorigenesis, and therefore may signal in a similar manner as has been reported for canonical activating mutant EGFR (15, 16). Collectively, these data demonstrate that the H2073-SVD and -ASV cell lines can grow independently of EGF while maintaining dependency on EGFR signaling pathway for survival, and more generally Ex20Ins activating mutants likely signal in a mechanistically analogous manner to Ex19del and L858R mutants despite structural differences.

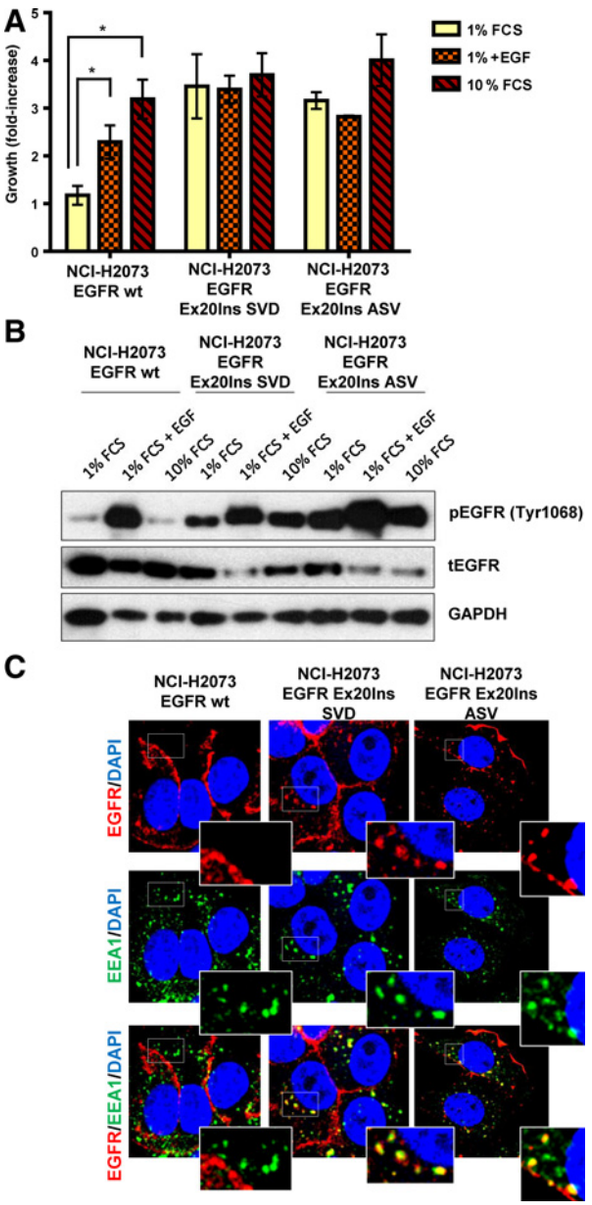

Figure 1.

EGFR Ex20Ins induce proliferation independent of EGF ligand and are constitutively internalized in endosomal compartment. **A,** Proliferation ($n = 3$; *, $P < 0.01$) and **B,** pEGFR and tEGFR level of the H2073-WT, H2073-SVD, and H2073-ASV cells grown in low (1%) serum with or without addition of EGF or in regular (10%) serum. **C,** Confocal sections of H2073-WT, H2073-SVD and H2073-ASV cells stained for EGFR (red), EEA1 (green) and DAPI (blue). Scale bar, 10 μm.

The most prevalent EGFR exon 20 insertions are sensitive to osimertinib *in vitro*

Next, we evaluated the potential of clinically relevant EGFR TKIs to suppress EGFR phosphorylation and proliferation *in vitro* of EGFR Ex20Ins mutant-expressing cells. Consistent with clinical observations, the first- and second-generation approved TKIs (gefitinib, erlotinib, and afatinib) showed high levels of potency against phosphorylation of the Ex20InsFQEA variant using the Cos-7 engineered cell line model (Fig. 2A), which importantly was recapitulated by the high potency levels of osimertinib and AZ5104 (Fig. 2A). Osimertinib and AZ5104 also potently inhibited phosphorylation of other EGFR Ex20Ins variants NPG, SVD, and ASV, and consistently exhibited greater relative potency compared to the reversible TKI erlotinib across each variant (Fig. 2A). Interestingly, the second-generation irreversible TKI afatinib similarly showed high activity against all the Ex20Ins variants (Fig. 2A). However, as with targeting T790M (13), compared to afatinib, osimertinib consistently displayed a greater level of activity towards Ex20Ins compared to wtEGFR, suggesting the superior wild-type sparing activity of osimertinib may enable greater levels of clinical target exposure to be achieved.

We then explored how the activity against Ex20Ins translated into cell proliferation inhibition. In line with the phosphorylation data, osimertinib (Fig. 2B; Supplementary Fig. S3A) and AZ5104 (Fig. 2C; Supplementary Fig. S3B) demonstrated similar potent levels of proliferation inhibition against H2073-FQEA, H2073-SVD, and H2073-ASV cell lines. However, in contrast to the pEGFR activity, osimertinib did not exhibit the same margin of selectivity between Ex20Ins and wtEGFR, although the source of this disconnect is unclear (e.g., differences in signaling thresholds). To put osimertinib data into context, both gefitinib and afatinib also showed high potency only against the clinically sensitive H2073-FQEA, which was also similar to their wtEGFR activity

A

Compounds	EGFR Ex20Ins NPG (COS7) IC_{50}	EGFR Ex20Ins SVD (COS7) IC_{50}	EGFR Ex20Ins ASV (COS7) IC_{50}	EGFR Ex20Ins FQEA (COS7) IC_{50}	EGFR WT (H2073) IC_{50}	EGFR Ex20Ins SVD (H2073) IC_{50}
Erlotinib	98 (*n* = 3) (36,264)	867.2 (*n* = 3) (279.7,2688.6)	1450.5 (*n* = 4) (635.7,3309.6	11.4 (*n* = 5) (8.4,15.4)	25.8 (*n* = 6) (14.2,46.8)	1273.6 (*n* = 4) (20.3,79793.8)
Afatinib	2.7 (*n* = 15) (1.9,4)	5.9 (*n* = 47) (5.0,6.8)	4.9 (*n* = 10) (3.7,6.5)	5.3 (*n* = 8) (3.6,7.8)	4.9 (*n* = 18) (3.0,8.0)	6.1 (*n* = 12) (4.6,8.1)
Osimertinib	6.2 (*n* = 3) (2.6,15.2)	59.6 (*n* = 3) (19.0,186.7)	28.7 (*n* = 3) (15.7,52.7)	13.9 (*n* = 6) (7.3,26.5)	470.1 (*n* = 8) (196.9,1122.2)	96.6 (*n* = 6) (55.5,168.3)
AZ5104	1.9 (*n* = 5) (1.4,2.5)	6.7 (*n* = 4) (4.0,11.4)	4.4 (*n* = 4) (3.7,5.3)	6.7 (*n* = 7) (4.8,9.2)	20.8 (*n* = 9) (14.8,29.2)	9.5 (*n* = 6) (3.9,22.9)

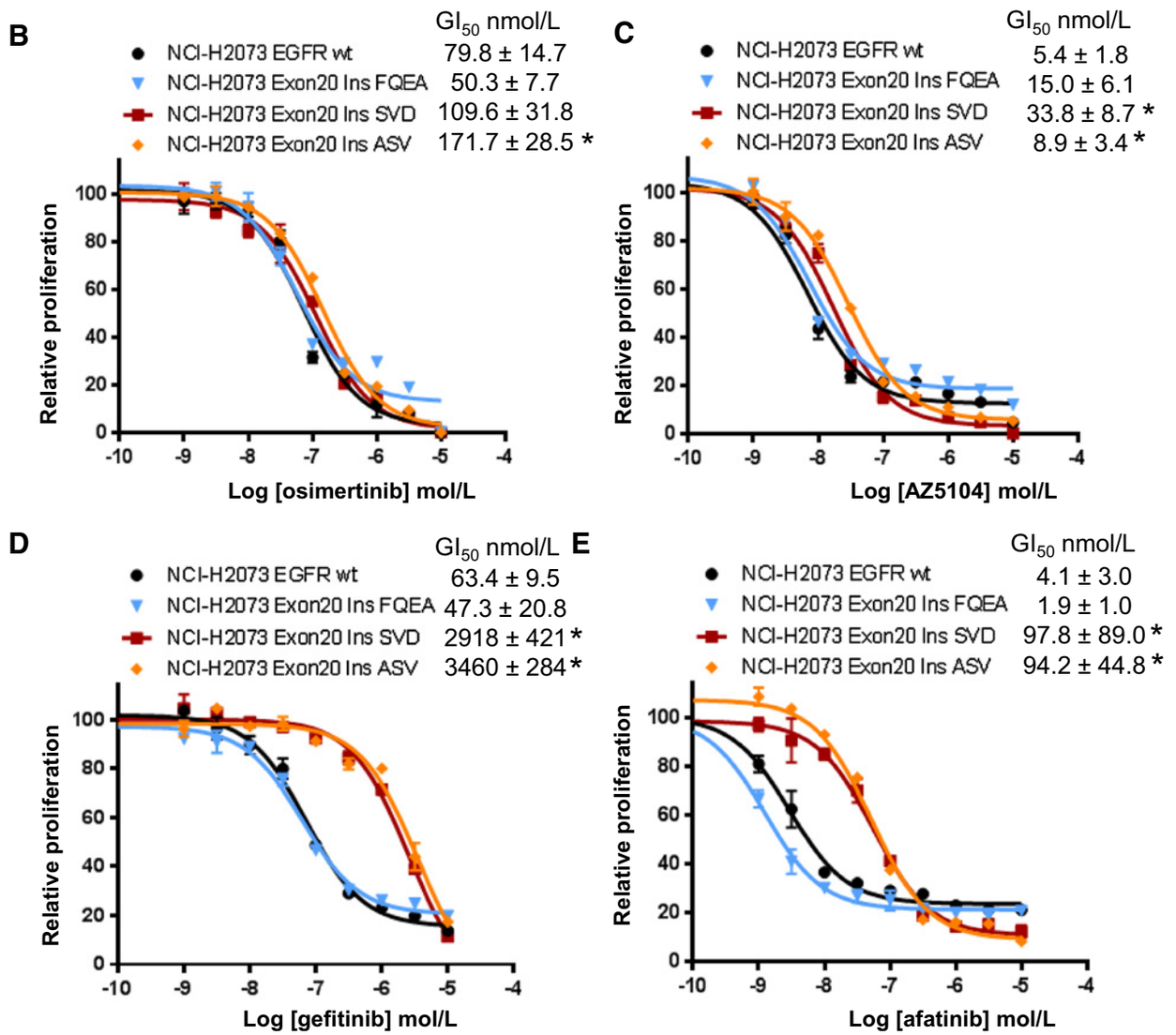

Figure 2.

Sensitivity of EGFR exon 20 insertion mutations to clinically relevant EGFR TKIs *in vitro*. **A,** Effect of TKI on the phosphorylation of various EGFR Ex20Ins *in vitro*. Data are represented as apparent geomean IC_{50} (nmol/L) values from at least two separate experiments expressed with 95% confidence intervals value in brackets. Effect of (**B**) osimertinib, (**C**) AZ5104, (**D**) gefitinib, and (**E**) afatinib used at the indicated concentrations on proliferation of H2073, H2073-SVD, and H2073-ASV cells. Proliferation was measured after 4 days of treatment and plotted relative to untreated controls. The data presented represent the results of a typical experiment, average values calculated from $n \geq 3 \pm$ SD (*, $P < 0.05$).

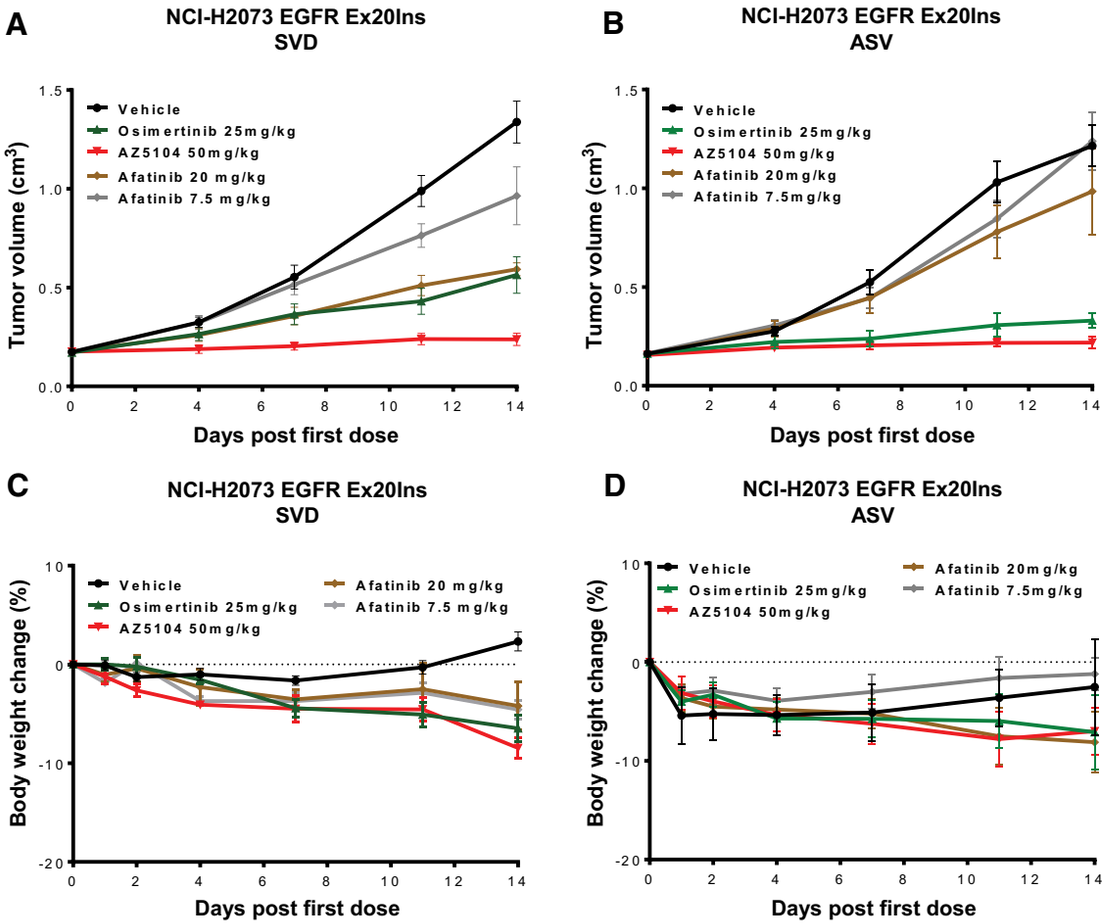

Figure 3.

Osimertinib and AZ5104 monotherapy induce tumor growth inhibition in both NSCLC H2073 Ex20Ins SVD and ASV xenograft models *in vivo*. Tumor growth inhibition following daily dosing of vehicle, osimertinib 25 mg/kg once daily, AZ5104 50 mg/kg once daily or afatinib 7.5 or 20 mg/kg once daily in the subcutaneous, (**A**) H2073-SVD or (**B**) H2073-ASV, xenograft model in CB17 SCID mice. **C** and **D,** No significant body weight loss (less than 10% of starting body weight) is observed at these efficacious doses. Data expressed as percentage change in CB17 SCID mouse body weight relative to start size on day 0. Data are represented as mean ± SEM ($n = 10$ for vehicle and $n = 5$ for osimertinib, AZ5104 and afatinib-treated groups.

(Fig. 2D and E). However, in important contrast to osimertinib, the earlier generation TKIs demonstrated significantly lower levels of activity against H2073-SVD and H2073-ASV cell lines compared to wtEGFR (Fig. 2D and E; Supplementary Fig. S3C and S3D).

Collectively these data suggest that osimertinib and its metabolite AZ5104 can effectively inhibit EGFR-phosphorylation and proliferation of cell lines carrying Ex20Ins mutations in EGFR, and have a more favorable mutant-selective profile compared to currently approved first- and second-generation TKIs.

Osimertinib and AZ5104 induce tumor growth inhibition to a greater degree than afatinib in EGFR Ex20Ins *in vivo* xenograft models

To explore the *in vivo* activity of osimertinib and its metabolite AZ5104, we administered the drugs as monotherapy against the two different NSCLC EGFR CRISPR-engineered H2073 xenografts that carry either the Ex20Ins SVD (D770_N771InsSVD) or Ex20Ins ASV (V769_D770InsASV). Consistent with clinical experience, the Ex20Ins SVD and ASV confer primary resistance to 7.5 mg/kg, a dose that represents the 40 mg clinical starting dose of afatinib (Fig. 3A and B). The H2073 parental cell line is sensitive to a similar dose of afatinib (Supplementary Fig. S4), indicating resistance is due to the Ex20Ins rather than the cell line background.

In contrast to the poor activity of clinically-relevant afatinib, once-daily administration of 25 mg/kg of osimertinib (a dose that approximates the clinically approved 80 mg dose) or the maximum tolerated dose of AZ5104, induced significant tumor growth inhibition in both the Ex20Ins SVD (65%, $P < 0.001$ and 95%, $P < 0.001$, respectively at day 14) and Ex20Ins ASV (82%, $P < 0.001$ and 95%, $P < 0.001$, respectively at day 14) xenograft models when compared to the control group (Fig. 3A and B). Both compounds were well tolerated and minimal body weight loss (less than 10% of starting body weight) was observed (Fig. 3C and D).

Osimertinib and AZ5104 inhibit EGFR phosphorylation and downstream signaling pathways *in vivo*

To explore the relationship between efficacy and target modulation, mice bearing H2073-SVD tumors were treated with a

single dose of either osimertinib, AZ5104, or afatinib and tumors were harvested 1, 6, 16, 24, and 30 hours later. Comprehensive EGFR pathway biomarkers were used to assess the impact of EGFR TKI within the tumor tissue. Pharmacodynamic effects were confirmed by assessing phospho-EGFR inhibition by ELISA (Fig. 4A; Supplementary Fig. S5A) and Western blot (Fig. 4B), and downstream signaling pathways inhibition by assessing phospho-AKT and phospho-ERK inhibition by immunoblotting (Fig. 4C and D; Supplementary Fig. S5B and S5C). Although in mice the pharmacokinetic half-life of osimertinib and AZ5104 is only approximately 3 hours (13), phospho-EGFR staining remained significantly diminished even after the 16 hour time point (Fig. 4A), consistent with their expected irreversible mode of action. Interestingly, although downstream signaling markers similarly showed maximal inhibition after 6 hours, in contrast with phospho-EGFR, they displayed more transient inhibition (Fig. 4C and D). Similar observations were made following afatinib administration. The stronger efficacy observed with AZ5104 when compared to osimertinib or afatinib correlated with a more profound and less transient inhibition of EGFR and downstream signaling pathways. Similar results were observed using the H2073-ASV (Supplementary Fig. S6A–S6C). These data demonstrate that both osimertinib and AZ5104 can achieve robust Ex20Ins-mediated pathway inhibition *in vivo* that is associated with tumor growth inhibition.

Osimertinib and AZ5104 are efficacious in EGFR Ex20Ins PDX models *in vivo*

Despite the compelling *in vitro* and *in vivo* activity observed in H2073 and Cos-7 models, these represent non-endogenous engineered systems. Therefore, we wished to evaluate activity using more directly relevant patient-derived xenograft (PDX) models. Strikingly, in a PDX model (LG1423) harboring the same prevalent EGFR Ex20ins V769_D770InsASV variant as used in H2073 studies, daily dosing of 25 mg/kg osimertinib induced a superior tumor growth inhibition than the higher 20 mg/kg dose of afatinib (60%, $P < 0.001$ and 18%, *P*: nonsignificant respectively at day 22) when compared to the control group (Fig. 5A). Similarly in a separate experiment, osimertinib induced superior tumor growth inhibition than erlotinib (93%, $P < 0.001$ and 15%, *P*: nonsignificant respectively at day 20) when compared to the control group (Fig. 5B). Despite experimental variability, osimertinib therefore consistently showed more meaningful efficacy compared to the earlier generation TKIs, at clinically relevant doses. Minimal body weight loss (less than 10% of starting body weight) was observed in these efficacy experiments (Supplementary Fig. S7A and S7B). The efficacy of osimertinib was associated with robust and sustained inhibition of phospho-EGFR and downstream signaling markers (Fig. 5C; Supplementary Fig. S8) following a single 25 mg/kg dose. Although both afatinib and erlotinib showed comparable pharmacodynamic effects following a single acute dose with respect to phospho-EGFR, inhibition of phospho-AKT and suppression of phospho-S6R at early timepoints appeared more robust with osimertinib compared to afatinib and erlotinib (Fig. 5C; Supplementary Fig. S8). Whether enhanced phospho-AKT inhibition and phospho-S6R suppression contributes to the improved activity of osimertinib is the subject of future studies.

We further examined tumor inhibition responses in two additional PDX models that carry less prevalent Ex20Ins variants (LXF2478; M766_A767insASV and LU0387; H773_V774insNPH). The LXF2478 model, resistant to a once-daily administration of afatinib (20 mg/kg) was sensitive to a once-daily administration of osimertinib (25 mg/kg) and AZ5104 (25 mg/kg) with 87% ($P < 0.001$) and 81% ($P < 0.001$) tumor growth inhibition respectively (measured at day 14), when compared to the control group (Fig. 5D). In the LU0387 model, once-daily administration of osimertinib (25 mg/kg) and AZ5104 (50 mg/kg for 7 days and 25 mg/kg for 7 days) induced 71% ($P < 0.001$) tumor growth inhibition and 86% regression ($P < 0.001$) respectively, at day 15 when compared to the control group (Fig. 5E). In a separate study, AZ5104 dosed at 25 mg/kg daily induced 7% regression ($P < 0.001$) at day 15 when compared to the control group (Supplementary Fig. S7C). Both compounds were well tolerated and minimal body weight loss was observed compared to pre-dose starting body weight (Supplementary Fig. S7D and S7E).

Collectively, these results demonstrate that osimertinib and its metabolite AZ5104 are highly active across a number of different Ex20Ins PDX models *in vivo* compared to afatinib, and further support the potential efficacy of osimertinib in patients harboring various EGFR Ex20Ins mutant tumors.

Discussion

Despite the success of approved EGFR TKI therapies in the treatment of EGFR-mutant NSCLC, the benefit from these agents remains mostly limited to patients diagnosed with the canonical common Ex19del and L858R mutant subtypes. Alongside L858R and Ex19del, Ex20Ins mutants account for the third most prevalent group of EGFR mutations, representing 4% to 10% of the segment. However, this Ex20Ins subgroup is largely refractory to current TKIs and remains a key area of unmet need requiring identification of new effective treatment options. To this end, we evaluated the activity of the next-generation EGFR TKI osimertinib and its metabolite AZ5104 across a variety of pre-clinical models representing the most frequently occurring EGFR Exon 20 insertions. Although a previous report has postulated the potential of osimertinib in the Ex20Ins setting (14), this study was limited to using *in vitro* Ba/F3 engineered cell models, and therefore we undertook a more comprehensive approach to evaluating osimertinib across more clinically relevant models with additional *in vivo* studies.

A key challenge with the Ex20Ins is the much more diverse nature of the mutational landscape, with more than 100 potential mutations identified, so it is not feasible to profile all possible Ex20Ins variants. Our primary strategy was to therefore focus the evaluation of osimertinib on the two most prevalent forms of Ex20Ins (D770_N771InsSVD and V769_D770InsASV), which account for approximately 40% of such patients (2, 4, 17). Our findings provide evidence that the two most clinically prevalent variants of Ex20Ins mutations, SVD (D770_N771InsSVD) and Ex20Ins ASV (V769_D770InsASV; refs. 2, 4, 17), are constitutively active in an analogous manner to canonical activating-mutations. Importantly, here we report pre-clinical activity of osimertinib and AZ5104 (a circulating metabolite of osimertinib; ref. 13), against these two most clinically prevalent variants of Ex20Ins mutations. Despite the mutant heterogeneity with EGFRex20Ins we propose that TKIs that can effectively target these prevalent mutations are likely to at least provide significant clinical benefit to this EGFR-mutant subset. In addition, we demonstrate activity against various less prevalent Ex20Ins mutations using engineered pre-clinical

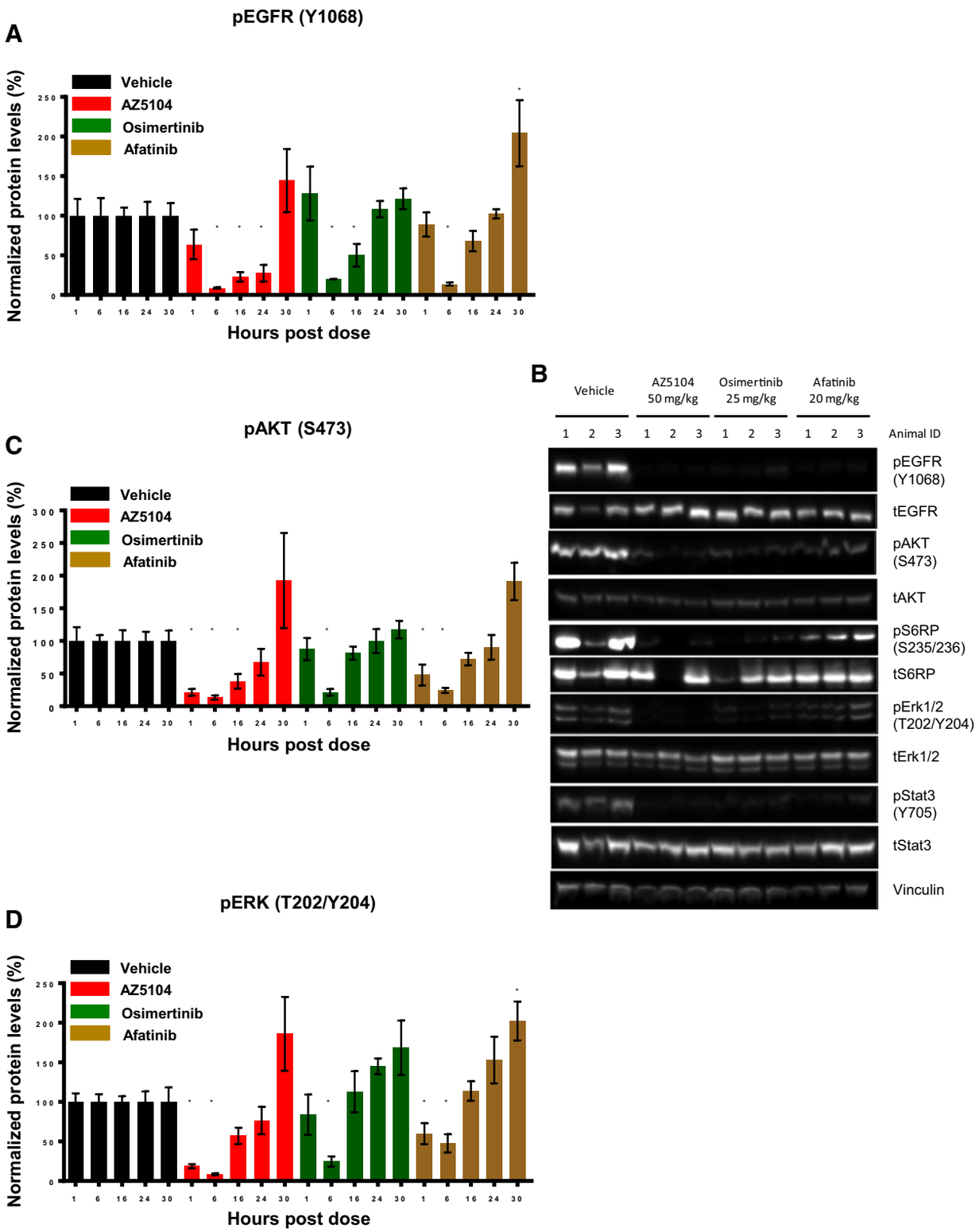

Figure 4.

Osimertinib and AZ5104 treatment results in strong inhibition of pEGFR and downstream signaling. **A,** Quantification of the ratio pEGFR: tEGFR determined by ELISA on tumors collected 1, 6, 16, 24, and 30 hours following one dose of either vehicle, osimertinib 25 mg/kg once daily, AZ5104 50 mg/kg once daily, or afatinib 7.5 or 20 mg/kg once daily. Data are represented as mean ± SEM ($n = 4$ for vehicle and treated groups). **B,** Immunoblot of representative individual tumors from the 6-hour time point with the indicated antibodies. **C,** Quantification of the level of pAKT or (**D**) pERK1/2 determined by immunoblot on tumors collected 1, 6, 16, 24, and 30 hours following one dose of either vehicle, osimertinib, AZ5104 or afatinib. Data are represented as mean ± SEM ($n = 4$ for vehicle and treated groups). *, $P < 0.05$.

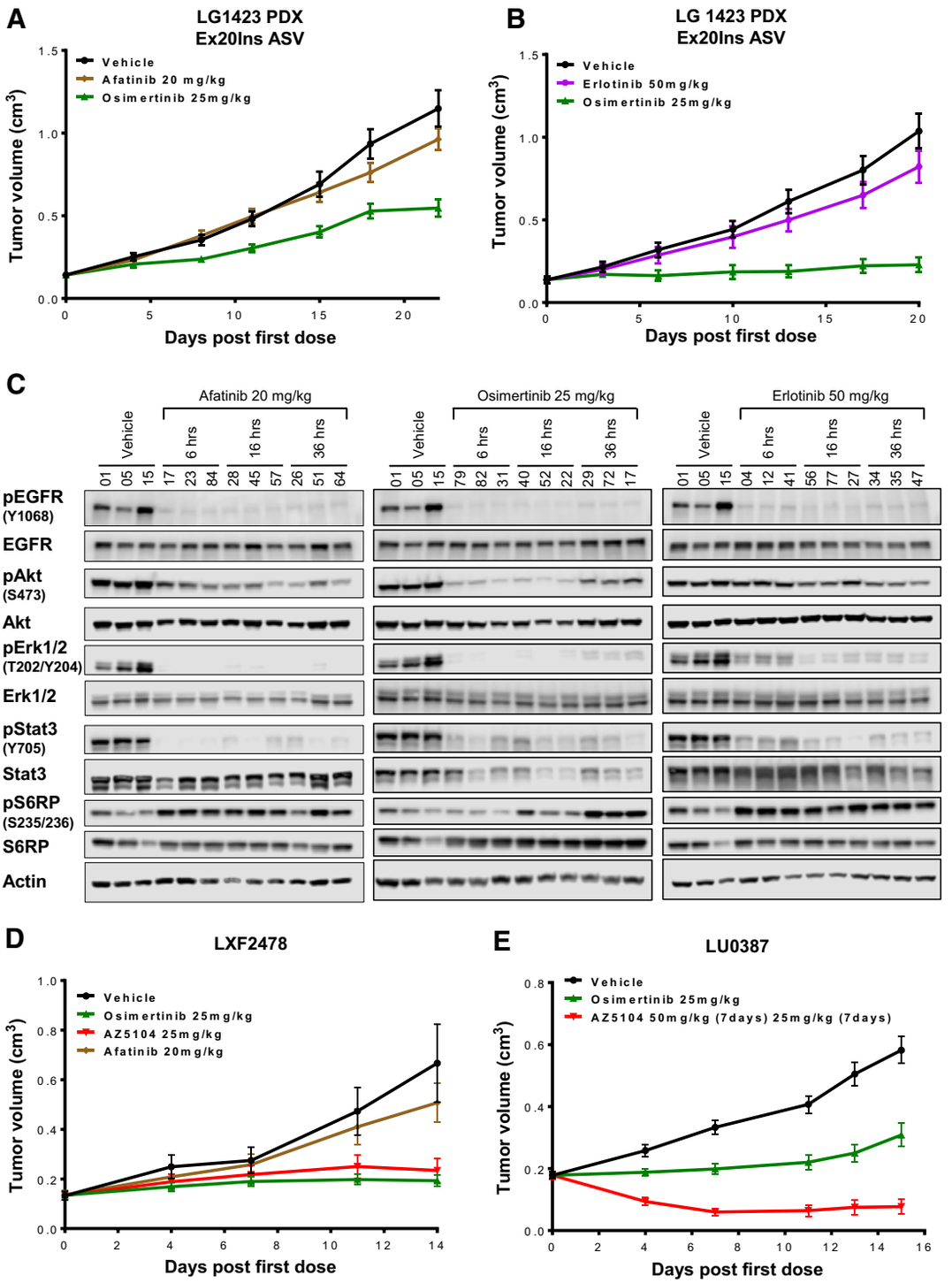

Figure 5.

Osimertinib and AZ5104 induce significant tumor growth inhibition in three PDX models carrying different Ex20Ins mutations. Tumor growth inhibition following no treatment or (**A**) daily dosing of osimertinib at 25 mg/kg and afatinib 20 mg/kg or (**B**) daily dosing of osimertinib at 25 mg/kg and erlotinib at 50 mg/kg in the subcutaneous PDX (LG1423) model harboring the V769_D770InsASV. **C,** Immunoblot of individual LG1423 tumors at relevant time points following a single dose of afatinib, osimertinib or erlotinib vs. no treatment. **D,** Tumor growth inhibition following daily dosing of vehicle, osimertinib at 25 mg/kg, AZ5104 at 25 mg/kg or afatinib at 20 mg/kg in the subcutaneous LXF2478 PDX model harboring the M766_A767insASV mutation. **E,** Tumor growth inhibition following daily dosing of vehicle, osimertinib at 25 mg/kg or AZ5104 at 50 mg/kg in the subcutaneous LU0387 PDX model harboring the H773_V774insNPH mutation.

models and PDXs, indicating wider potential to target multiple variant forms.

Given the lack of available endogenous cell line models, we utilized CRISPR editing technology to convert NCI-H2073 cells which express wild-type EGFR into cell lines homogenously expressing each of the two most prevalent Ex20Ins mutants. Using this approach, we were able to demonstrate for the first time in a disease-relevant cellular context that these prevalent mutations are sufficient to confer dependence of NSCLC cells on ligand-independent EGFR signaling, accompanied by hallmarks of the more common EGFR mutations such as constitutive receptor phosphorylation and receptor endosomal internalization. Taken together, these studies support the notion that Ex20Ins mutations have many similar signaling and cell biology characteristics as common activating mutants, despite their disparate mutational changes. However, further exploratory studies are needed to better understand the molecular mechanisms related to Ex20Ins biology and comparison to other activating mutations.

Using *in vitro* phospho-EGFR studies, osimertinib and its active metabolite AZ5104 effectively inhibited Ex20Ins mutant forms of EGFR, at potencies comparable to the common activating and T790M mutants previously published (13). Osimertinib was designed to have selective activity against common activating and T790M mutants compared to wild-type EGFR. Although Ex20Ins mutants lack T790M-associated structural differences proximate to the ATP-binding site (7), the mutant-selective profile of osimertinib appeared to remain for Ex20Ins variants, in contrast to the other TKIs. The wild-type EGFR activity of TKIs is believed to be a key factor limiting the achievable clinical exposures against the mutant EGFR target, and therefore may impact clinical benefit. It is therefore notable that although afatinib similarly showed high levels of phospho-EGFR potency across the Ex20Ins variants *in vitro*, it also similarly displayed much higher level of potency against wt-EGFR when compared to osimertinib.

The consequence of wild-type margins is further supported from the subsequent *in vitro* proliferation studies. Interestingly, the margin of selectivity between Ex20Ins mutants and wtEGFR observed in pEGFR assays is not apparent for osimertinib in the more chronic proliferation assays, and the reason for this remains unclear, although it could be due to differences in signaling thresholds between the cell lines. Nevertheless, it is notable that both afatinib and gefitinib harbor very similar potencies between wtEGFR and the FQEA variant which has been demonstrated to be sensitive to these TKIs clinically. However, proliferation activity is much lower against the other prevalent Ex20Ins variants compared to wtEGFR for these TKIs. This data provides a useful benchmark and further supports the notion that it is the balance of activity between mutant EGFR and wtEGFR that is important for driving clinical benefit, that is, benefit is only seen in FQEA in which the wtEGFR pharmacology is not the primary limiting activity. In this regard, whereas other TKIs show a significant drop-off in potency from wtEGFR towards the prevalent Ex20Ins forms, suggesting that wtEGFR activity maybe more dose-limiting, osimertinib retains a more comparable balance of potency between wtEGFR and all Ex20Ins mutations. Taken together, the *in vitro* data supports the premise that dose-limiting toxicities related to nonselective inhibition of wild-type EGFR may have greater impact on limiting the effectiveness of afatinib across Ex20Ins variants compared to osimertinib, although it remains structurally unclear how osimertinib retains a more advantageous selectivity against wild-type in Ex20Ins setting.

The circulating metabolite AZ5104 also demonstrated potent activity, suggesting it could potentially contribute to the overall efficacy of osimertinib, although the clinical relevance remains unclear since the metabolite only exists at ~10% of parental levels (18).

To investigate how osimertinib and metabolite potency translated to *in vivo* efficacy, the modified H2073 models were established as xenografts. *In vivo*, osimertinib delivered high levels of antitumor activity across both Ex20Ins models at 25 mg/kg/day, a dose modeled to be approximately consistent with the 80 mg clinically-approved dose for targeting T790M tumors. Moreover, the level of efficacy achieved was significantly greater than clinically relevant doses of afatinib. Consistent with *in vitro* pharmacology, the AZ5104 metabolite was similarly able to achieve high levels of tumor inhibition. The tumor inhibition activity of both osimertinib and AZ5104 was associated with potent mechanistic activity against EGFR target and downstream signaling pathways, although the transient nature of pathway suppression may imply that more durable inhibition would be required to achieve robust tumor shrinkage in these models. Finally, to evaluate activity in Ex20Ins models that more directly mimic the clinical setting, we tested these TKIs in three separate PDX models. Most notably, we demonstrated superior tumor inhibition activity of osimertinib compared to erlotinib and afatinib in a PDX harboring one of the most common EGFR Exon 20 insertions (V769_D770InsASV), consistent with the H2073 model harboring the same insert variant. Furthermore, in two other PDX models harboring less prevalent Ex20ins, osimertinib similarly delivered high levels of antitumor activity compared to afatinib (M766_A767insASV; H773_V774insNPH). These data are the first to demonstrate that osimertinib can achieve superior growth inhibition across diverse Ex20Ins PDX models at clinically relevant doses *in vivo* compared to afatinib. However, it is noteworthy that despite the encouraging levels of tumor growth inhibition, osimertinib at the maximally tolerated preclinical dose of 25 mg/kg is not able to achieve the same levels of shrinkage observed across *in vivo* models representing canonical EGFR activating and T790M mutants (14). Further work will be required to better understand whether this more limited preclinical efficacy is related to the inherent background of the models being used, differences in the biology of Ex20Ins and/or the limitations of preclinical dosing and PK levels. However, the lower *in vitro* potency and reduced tumor growth inhibition of osimertinib against Ex20Ins mutant models compared to common activating mutants may suggest that increased dose levels (e.g., 160 mg osimertinib; ref. 19) may be required clinically. The question of optimal dose levels against Ex20Ins tumors in the clinical setting can only be explored empirically in the clinic, given the limitation of preclinical doses that can be achieved (i.e., 160 mg clinical dose cannot be recapitulated in preclinical studies).

Taken together, the work presented herein provides a comprehensive preclinical *in vitro* and *in vivo* evaluation of osimertinib compared to other approved TKIs in this segment. Consistent with the previous report (12), our data supports osimertinib as having a differentiated profile compared to earlier generation TKIs: (i) high *in vitro* potency across a range of Ex20Ins variants, (ii) evidence for a more consistent and favorable wtEGFR margin of selectivity, and (iii) superior efficacy across a range of xenograft and PDX models at clinically relevant doses. Although additional

pre-clinical studies are warranted to further our understanding of Ex20Ins biology and response to TKIs such as osimertinib across this diverse mutational landscape, these studies have limitations for fully predicting clinical benefit and moreover are not able to fully recapitulate multiple complexities such as PK differences, metabolite contribution, dosing levels, etc. We therefore propose that empirical clinical studies will be required to fully evaluate the potency of osimertinib across the diverse Ex20Ins mutation landscape and inform optimal dosing. Overall, we suggest the work presented here provides sufficient evidence to warrant the clinical testing of osimertinib within this EGFR activating-mutant Ex20Ins population to establish whether osimertinib can offer improved clinical benefit in this important remaining area of unmet need as a differentiated next generation TKI.

Disclosure of Potential Conflicts of Interest

J.W. Riess is a consultant/advisory board member of Takeda. M.R.V. Finlay has ownership interest (including patents) from AstraZeneca Stock. D.R. Gandara is a consultant/advisory board member of AstraZeneca. P.C. Mack is a consultant/advisory board member of AstraZeneca. No potential conflicts of interest were disclosed by the other authors.

Authors' Contributions

Conception and design: N. Floc'h, M.J. Martin, J.W. Riess, R.A. Ward, M.R.V. Finlay, D. McKerrecher, D.R. Gandara, P.C. Mack, D.A.E. Cross
Development of methodology: N. Floc'h, M.J. Martin, J.W. Riess, J.P. Orme, L. Ménard, D.J. O'Neill, P.C. Mack
Acquisition of data (provided animals, acquired and managed patients, provided facilities, etc.): N. Floc'h, J.W. Riess, J.P. Orme, A.D. Staniszewska, L. Ménard, D.J. O'Neill, M. Cheng, J.G. Keck, D.R. Gandara, P.C. Mack
Analysis and interpretation of data (e.g., statistical analysis, biostatistics, computational analysis): N. Floc'h, M.J. Martin, J.W. Riess, J.P. Orme, A.D. Staniszewska, L. Ménard, M.E. Cuomo, D.J. O'Neill, R.A. Ward, M.R.V. Finlay, M. Cheng, D.P. Vang, P.C. Mack, D.A.E. Cross
Writing, review, and/or revision of the manuscript: N. Floc'h, M.J. Martin, J.W. Riess, J.P. Orme, M.E. Cuomo, D.J. O'Neill, R.A. Ward, M.R.V. Finlay, D. McKerrecher, M. Cheng, D.P. Vang, D.R. Gandara, P.C. Mack, D.A.E. Cross
Administrative, technical, or material support (i.e., reporting or organizing data, constructing databases): N. Floc'h, M.J. Martin, J.W. Riess, R.A. Ward, M. Cheng, R.A. Tsai, P.C. Mack
Study supervision: N. Floc'h, J.W. Riess, D.R. Gandara, D.A.E. Cross
Other (generated CRISPR lines): M.E. Cuomo
Other (project leader): D. McKerrecher

Acknowledgments

The authors would like to thank Susan Ashton for her precious advice on how to evaluate osimertinib and AZ5104 *in vivo*; Beverley Hammond, Martine Mellor, Paula Taylor, Amar Rahi, and Staff in Laboratory Animal Sciences in Alderley Park for technical support; Marcello Maresca and Harriet Andersen for designing, generating, and providing the vector for genome editing; Beate Frank for statistical support.

Support was provided by a Paul Calabresi Career Development Award in Clinical Oncology National Institutes of Health Grant 5 K12 CA 138464 (J.W. Riess) and by the Molecular Pharmacology Shared Resource, UC Davis Comprehensive Cancer Center Support Grant NCI P30CA093373.

The costs of publication of this article were defrayed in part by the payment of page charges. This article must therefore be hereby marked *advertisement* in accordance with 18 U.S.C. Section 1734 solely to indicate this fact.

Received August 8, 2017; revised December 1, 2017; accepted February 7, 2018; published first February 26, 2018.

References

1. Sharma SV, Bell DW, Settleman J, Haber DA. Epidermal growth factor receptor mutations in lung cancer. Nat Rev Cancer 2007;7:169–81.
2. Arcila ME, Nafa K, Chaft JE, Rekhtman N, Lau C, Reva BA, et al. EGFR exon 20 insertion mutations in lung adenocarcinomas: prevalence, molecular heterogeneity, and clinicopathologic characteristics. Mol Cancer Ther 2013; 12:220–9.
3. Oxnard GR, Lo PC, Nishino M, Dahlberg SE, Lindeman NI, Butaney M, et al. Natural history and molecular characteristics of lung cancers harboring EGFR exon 20 insertions. J Thorac Oncol 2013;8:179–84.
4. Yasuda H, Kobayashi S, Costa DB. EGFR exon 20 insertion mutations in non-small-cell lung cancer: preclinical data and clinical implications. Lancet Oncol 2012;13:e23–31.
5. Chen D, Song Z, Cheng G. Clinical efficacy of first-generation EGFR-TKIs in patients with advanced non-small-cell lung cancer harboring EGFR exon 20 mutations. Onco Targets Ther 2016;9:4181–6.
6. Naidoo J, Sima CS, Rodriguez K, Busby N, Nafa K, Ladanyi M, et al. Epidermal growth factor receptor exon 20 insertions in advanced lung adenocarcinomas: Clinical outcomes and response to erlotinib. Cancer 2015;121:3212–20.
7. Yasuda H, Park E, Yun CH, Sng NJ, Lucena-Araujo AR, Yeo WL, et al. Structural, biochemical, and clinical characterization of epidermal growth factor receptor (EGFR) exon 20 insertion mutations in lung cancer. Sci Transl Med 2013;5:216ra177.
8. Yang JC, Sequist LV, Geater SL, Tsai CM, Mok TS, Schuler M, et al. Clinical activity of afatinib in patients with advanced non-small-cell lung cancer harbouring uncommon EGFR mutations: a combined post-hoc analysis of LUX-Lung 2, LUX-Lung 3, and LUX-Lung 6. Lancet Oncol 2015;16:830–8.
9. Riess JW FG, Chen M, Lara PN, Kelly K, Peled N, Bufill JA, et al. Genomic profiling and PDX modeling of NSCLC with EGFR exon 20 insertions supports osimertinib based dual EGFR-blockade strategies. Proceedings of the 17th World Conference on Lung Cancer. Messe Wien Exhibition and Congress Center, Messeplatz 1, Postfach 277 A-1021, Vienna, Austria, December 4-7, 2016.
10. Siegel RL, Miller KD, Jemal A. Cancer Statistics, 2017. CA Cancer J Clin 2017;67:7–30.
11. Kris MG, Johnson BE, Berry LD, Kwiatkowski DJ, Iafrate AJ, Wistuba II, et al. Using multiplexed assays of oncogenic drivers in lung cancers to select targeted drugs. JAMA 2014;311:1998–2006.
12. Finlay MR, Anderton M, Ashton S, Ballard P, Bethel PA, Box MR, et al. Discovery of a potent and selective EGFR inhibitor (AZD9291) of both sensitizing and T790M resistance mutations that spares the wild type form of the receptor. J Med Chem 2014;57:8249–67.
13. Cross DA, Ashton SE, Ghiorghiu S, Eberlein C, Nebhan CA, Spitzler PJ, et al. AZD9291, an irreversible EGFR TKI, overcomes T790M-mediated resistance to EGFR inhibitors in lung cancer. Cancer Discov 2014;4: 1046–61.
14. Hirano T, Yasuda H, Tani T, Hamamoto J, Oashi A, Ishioka K, et al. In vitro modeling to determine mutation specificity of EGFR tyrosine kinase inhibitors against clinically relevant EGFR mutants in non-small-cell lung cancer. Oncotarget 2015;6:38789–803.
15. Vieira AV, Lamaze C, Schmid SL. Control of EGF receptor signaling by clathrin-mediated endocytosis. Science 1996;274:2086–9.
16. Wang Y, Pennock S, Chen X, Wang Z. Endosomal signaling of epidermal growth factor receptor stimulates signal transduction pathways leading to cell survival. Mol Cell Biol 2002;22:7279–90.
17. Pan Y, Zhang Y, Li Y, Hu H, Wang L, Li H, et al. Prevalence, clinicopathologic characteristics, and molecular associations of EGFR exon 20 insertion mutations in East Asian patients with lung adenocarcinoma. Ann Surg Oncol 2014;21Suppl 4:S490–6.
18. Planchard D, Brown KH, Kim DW, Kim SW, Ohe Y, Felip E, et al. Osimertinib Western and Asian clinical pharmacokinetics in patients and healthy volunteers: implications for formulation, dose, and dosing frequency in pivotal clinical studies. Cancer Chemother Pharmacol 2016; 77:767–76.
19. Janne PA, Yang JC, Kim DW, Planchard D, Ohe Y, Ramalingam SS, et al. AZD9291 in EGFR inhibitor-resistant non-small-cell lung cancer. N Engl J Med 2015;372:1689–99.